Progress In Electromagnetics Research, PIER 52, 129–151, 2005

A LOW-ORDER-SINGULARITY ELECTRIC-FIELD INTEGRAL EQUATION SOLVABLE WITH PULSE BASIS FUNCTIONS AND POINT MATCHING

R. A. Shore and A. D. Yaghjian

Air Force Research Laboratory/SNHA
Hanscom AFB, MA 01731, USA

Abstract—The conventional form of the electric-field integral equation (EFIE), unlike the magnetic-field integral equation, cannot be solved accurately with the method of moments using pulse basis functions and point matching. A new form of the EFIE is derived whose kernel has no greater singularity than that of the free-space Green's function. This low-order-singularity form of the EFIE, the LEFIE, is solved numerically for perfectly electrically conducting bodies of revolution (BORs) using pulse basis functions and point-matching. Derivatives of the current are approximated with finite differences using a quadratic Lagrangian interpolation polynomial. Such a simple solution of the LEFIE is contingent, however, upon the vanishing of a linear integral that appears when the original EFIE is transformed to obtain the LEFIE. This generally restricts the applicability of the LEFIE to smooth closed scatterers. Bistatic scattering calculations performed for a prolate spheroid demonstrate that results comparable in accuracy to those of the conventionally solved EFIE can be obtained with the LEFIE using pulse basis functions and point matching provided a higher density of points is used close to the ends of the BOR.

1. INTRODUCTION

There are numerous commercial codes available that numerically solve electric-field integral equations (EFIEs) for the current and scattered fields produced by an electromagnetic wave incident on a perfectly electrically conducting (PEC) scatterer. For research purposes and for certain specialized geometries, however, it is often advantageous to have the flexibility and control inherent in writing one's own computer program. By far, the simplest approach for numerically solving integral equations is to use the method of moments (MOM) with pulse basis functions and point matching. Unfortunately, the EFIE, unlike the magnetic-field integral equation (MFIE), cannot be solved accurately using pulse basis functions and point matching (as demonstrated in Figure 4 below), and thus considerably more effort is required to write a computer code for numerically solving the EFIE. (It can be shown that it is primarily the higher order singularity of the EFIE kernel, rather than the derivatives of the current, that prevents an accurate solution using pulse basis functions and point matching.) For open scatterers or many thin bodies, the solution to the MFIE is indeterminate or unstable, respectively, and it becomes necessary to use the EFIE. Moreover, because confidence in numerical solutions is greatly enhanced by having two independent numerical solutions that agree to within a certain accuracy, it is often highly desirable to obtain the solution to the EFIE even if the MFIE is also applicable.

The main purpose of this paper is to derive a low-order-singularity electric-field integral equation (LEFIE) that can be accurately solved using the MOM with pulse basis functions and point matching. This LEFIE, whose kernel, like that of the MFIE, has no singularity greater than that of the free-space Green's function, is solved numerically for perfectly conducting bodies of revolution (BORs) using pulse

basis functions and point matching. Derivatives of the current are approximated with finite differences using a quadratic Lagrangian interpolation polynomial. This simple solution of the LEFIE is contingent, however, upon the vanishing of a line integral that appears when the original EFIE is transformed to obtain the LEFIE. This requirement generally restricts the simple applicability of the LEFIE to smooth closed surfaces.

Bistatic scattering calculations performed for scattering of a plane wave by a prolate spheroid demonstrate that numerical results comparable in accuracy to those of the conventionally solved EFIE can be obtained with the LEFIE using pulse basis functions and point matching, provided a higher density of points is used close to the ends of the BOR generating curve to compensate for the use of one-sided finite difference approximations of the first and second derivatives of the current.

The paper is organized as follows. Section 2 contains the derivation and analysis of the low-order-singularity electric-field integral equation especially as it is applied to BOR scattering problems. It is divided into four subsections beginning with the derivation of the general LEFIE in Subsection 2.1 and its restatement for a BOR in Subsection 2.2. The solution of the LEFIE for a closed BOR using pulse basis functions and point matching is outlined in Subsection 2.3. In Appendix A detailed expressions are given for 1) the elements of the Z matrices that multiply the column vectors of the surface current expansion function coefficients to be determined, 2) the elements of the $\mathbf{V}$ column vectors in the right-hand side of the matrix equation formulation of the LEFIE, 3) the currents induced on the surface of a BOR by a transverse electric (TE) and transverse magnetic (TM) linearly polarized plane wave in terms of the solution to the LEFIE matrix equation, and 4) the components of the far scattered electric field. Subsection 2.4 determines the number of angular Fourier modes required to accurately compute the induced current and scattered fields for a BOR.

Section 3 contains the numerical results of calculations performed with a computer program written to implement and validate the solution of the LEFIE formulated in Section 2 for a BOR. The paper concludes with a brief summary in Section 4.

2. ANALYSIS

2.1. Derivation of the Low-Order-Singularity Electric-Field Integral Equation

We begin the derivation of the LEFIE with the conventional form of the EFIE for the surface current $\mathbf{K}(\mathbf{r})$ on the surface S of a PEC scatterer [1]:

$$j\hat{\mathbf{n}}\times\oint_S \left[k^2\mathbf{K}(\mathbf{r}')G(\mathbf{r},\mathbf{r}') - \left(\nabla'_S\cdot\mathbf{K}(\mathbf{r}')\right)\nabla'G(\mathbf{r},\mathbf{r}')\right]dS' = \frac{k}{Z_0}\hat{\mathbf{n}}\times\mathbf{E}^{inc}(\mathbf{r}). \tag{1}$$

Here $G(\mathbf{r},\mathbf{r}')$ is the free-space Green's function for harmonic time dependence $\exp(j\omega t)$ with the frequency $\omega > 0$. That is

$$G(\mathbf{r},\mathbf{r}') = \frac{\exp(-jk\mid\mathbf{r}-\mathbf{r}'\mid)}{4\pi\mid\mathbf{r}-\mathbf{r}'\mid} \tag{2}$$

where $\mathbf{r}$ and $\mathbf{r}'$ are the vectors to the field and source points respectively, $\mathbf{K}(\mathbf{r}')$ is the electric current on S to be determined, μ_0 and ϵ_0 are the permeability and permittivity of free space respectively, $k = \omega/c$ with c the speed of light in free space, $Z_0 = (\mu_0/\epsilon_0)^{1/2}$ is the free-space impedance, and the operator $\nabla'_S\cdot$ is the surface divergence [2, Appendix 2, 18]. The incident electric field is denoted by $\mathbf{E}^{inc}(\mathbf{r})$ and $\hat{\mathbf{n}}$ is the unit normal out of the surface S at the position $\mathbf{r}$.

The "○" on the integral sign in (1) indicates that a small "principal area" isolates the singularity of the Green's function from the surface integration. The form of the EFIE in (1) is conditional upon the choice of the principal area being a circle with the singular point at its center (or another principal area that is adequately symmetric with respect to the singular point) [3].

The gradient operator acting on the free-space Green's function in (1) results in a higher order singularity, $1/\mid\mathbf{r}-\mathbf{r}'\mid^2$, instead of the $1/\mid\mathbf{r}-\mathbf{r}'\mid$ singularity for the free-space Green's function itself. What we want to do is to recast the conventional form of the EFIE into a new form that has no singularity higher than that of the free-space Green's function. To do this we begin by writing the gradient operating on the free-space Green's function as the sum of the surface gradient ∇'_S and the gradient in the normal direction so that (1) becomes

$$j\hat{\mathbf{n}}\times\oint_S [k^2\mathbf{K}(\mathbf{r}')G(\mathbf{r},\mathbf{r}') - \left(\nabla'_S\cdot\mathbf{K}(\mathbf{r}')\right)\nabla'_S G(\mathbf{r},\mathbf{r}') - \left(\nabla'_S\cdot\mathbf{K}(\mathbf{r}')\right)\frac{\partial G(\mathbf{r},\mathbf{r}')}{\partial n'}\hat{\mathbf{n}}']dS' = \frac{k}{Z_0}\hat{\mathbf{n}}\times\mathbf{E}^{inc}(\mathbf{r}). \tag{3}$$

The term in (3) with the normal derivative of G includes the cross product $\hat{\mathbf{n}} \times \hat{\mathbf{n}}'$ and does not have a singularity higher than G itself at $\mathbf{r} = \mathbf{r}'$. Focusing on the surface gradient term, we use the vector identity [2, Appendix 2, 26]

$$\nabla_S(AB) = A\nabla_S B + B\nabla_S A \tag{4}$$

to write

$$(\nabla'_S \cdot \mathbf{K})\nabla'_S G = \nabla'_S[(\nabla'_S \cdot \mathbf{K})G] - G\nabla'_S(\nabla'_S \cdot \mathbf{K}). \tag{5}$$

Using a Gauss integral theorem [2, Appendix 2, 43], we then obtain

$$\oint_S \nabla'_S[(\nabla'_S \cdot \mathbf{K})G]dS' = -\oint_S J'(\nabla'_S \cdot \mathbf{K})G\hat{\mathbf{n}}'dS' + \int_C (\nabla'_S \cdot \mathbf{K})G\hat{\mathbf{m}}'|dc'|. \tag{6}$$

In (6)

$$J' = \frac{1}{R'_1} + \frac{1}{R'_2} \tag{7}$$

where R'_1 and R'_2 are the principal radii of curvature at the surface point $\mathbf{r}'$, and C is a set of closed curves (defined below) on the surface of the PEC scatterer. The unit vector $\hat{\mathbf{m}}'$, defined at each point on the curves comprising C, is in the tangent plane to the surface at the point and perpendicular to the curve.

Since (6) is the key step in obtaining a new form of the EFIE it is important to understand the meaning of S and C in applying it. We assume that the surface S of a general PEC scatterer can be divided into a finite number of open subsurfaces sharing bounding curves in common with one another, such that on each subsurface the surface charge density $\sigma(\mathbf{r}') = -1/(j\omega)\nabla'_S \cdot \mathbf{K}(\mathbf{r}')$, its surface derivative, and J' are continuous and integrable, and $\hat{\mathbf{n}}'$ and $\hat{\mathbf{m}}'$ are continuous. In applying (6) to the surface S of the PEC scatterer, S is to be regarded as the superposition of these subsurfaces, and the surface and line integrations are performed separately for each subsurface with its bounding curve. The set of bounding curves comprise C. The unit vector $\hat{\mathbf{m}}'$ on each of the bounding curves comprising C points away from the subsurface it encloses. The surface of a closed finite cylinder, for example, is to be regarded as the superposition of three subsurfaces, the side cylindrical surface and the two end disks. The surface of a sphere, a simple smooth scatterer, can be regarded as the superposition of two hemispheres.

Combining (3) and (6) we obtain a new form of the EFIE with a

self-term singularity equal to that of the free-space Green's function

$$j\hat{\mathbf{n}}\times\oint_S \Big\{ \Big[k^2\mathbf{K}(\mathbf{r}') + \nabla'_S\left(\nabla'_S\cdot\mathbf{K}(\mathbf{r}')\right) + J'\left(\nabla'_S\cdot\mathbf{K}(\mathbf{r}')\right)\hat{\mathbf{n}}'\Big] G(\mathbf{r},\mathbf{r}') - \left(\nabla'_S\cdot\mathbf{K}(\mathbf{r}')\right)\frac{\partial G(\mathbf{r},\mathbf{r}')}{\partial n'}\hat{\mathbf{n}}'\Big\} dS' - j\hat{\mathbf{n}}\times\int_C \left(\nabla'_S\cdot\mathbf{K}(\mathbf{r}')\right) G(\mathbf{r},\mathbf{r}')\hat{\mathbf{m}}'|dc'|$$

$$= \quad \frac{k}{Z_0}\hat{\mathbf{n}}\times\mathbf{E}^{inc}(\mathbf{r}) \tag{8}$$

which, unlike the original EFIE in (1), is not conditional upon the shape of the principal area used to isolate the singularity of the Green's function.

Now our recasting of the conventional EFIE (1) into this new low-order-singularity form (8) is motivated by the desire to be able to solve the EFIE with the method of moments using pulse basis functions and point matching. Therefore we would like to avoid the line integral over C in (8). Assume that the surface S of the scatterer is closed and smooth enough so that $\sigma(\mathbf{r}') = -1/(j\omega)\nabla'_S\cdot\mathbf{K}(\mathbf{r}')$, its surface derivative, and J' are continuous and bounded, and $\hat{\mathbf{n}}'$ and $\hat{\mathbf{m}}'$ are continuous over S. Then (8) can be applied to any two contiguous open surfaces (with a smooth bounding curve) comprising the closed surface, the two line integrals over the common bounding curve of the two contiguous surfaces cancel, and (8) reduces to

$$j\hat{\mathbf{n}}\times\oint_S \Big\{ \Big[k^2\mathbf{K}(\mathbf{r}') + \nabla'_S\left(\nabla'_S\cdot\mathbf{K}(\mathbf{r}')\right) + J'\left(\nabla'_S\cdot\mathbf{K}(\mathbf{r}')\right)\hat{\mathbf{n}}'\Big] G(\mathbf{r},\mathbf{r}') - \left(\nabla'_S\cdot\mathbf{K}(\mathbf{r}')\right)\frac{\partial G(\mathbf{r},\mathbf{r}')}{\partial n'}\hat{\mathbf{n}}'\Big\} dS' = \frac{k}{Z_0}\hat{\mathbf{n}}\times\mathbf{E}^{inc}(\mathbf{r}). \tag{9}$$

If the scatterer has an open surface, edges, tips, or any boundary where σ or J' become singular or discontinuous, or $\hat{\mathbf{n}}'$ and $\hat{\mathbf{m}}'$ become discontinuous, the line integral over C cannot, in general, be omitted and the numerical solution to the LEFIE in (8) may be more complicated than that of the original EFIE. *Accordingly we will restrict our treatment of the LEFIE in this paper to PEC scatterers with closed smooth surfaces such as spheroids for which σ, its surface derivative, and J' are continuous and bounded, and $\hat{\mathbf{n}}'$ and $\hat{\mathbf{m}}'$ are continuous, so that the line integral over C can be omitted and the LEFIE takes the form (9).*

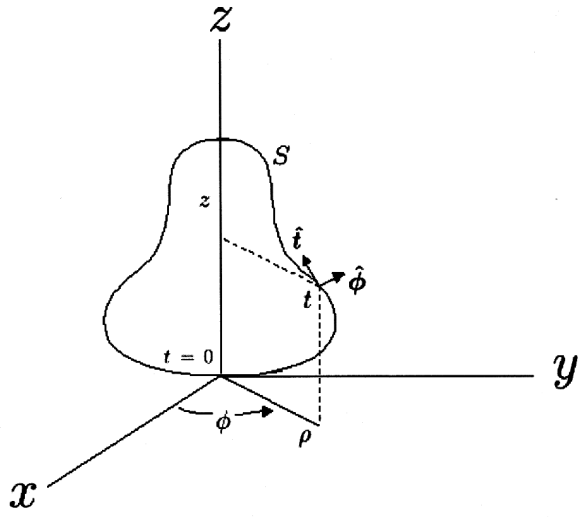

Figure 1. Body of revolution and coordinate system.

2.2. LEFIE for a BOR

We seek to determine the surface current and the far scattered field of a perfectly electrically conducting (PEC) closed body of revolution (BOR) excited by an incident plane wave. The geometry of the BOR is shown in Figure 1. Circular cylinder coordinates (ρ, ϕ, z) are employed with $(\hat{\boldsymbol{\rho}}, \hat{\boldsymbol{\phi}}, \hat{\mathbf{z}})$ denoting the corresponding unit vectors, and with the z axis chosen as the axis of revolution. The origin of the circular cylindrical coordinate system lies on the z axis but does not necessarily coincide with the lower pole of the BOR as in Figure 1. The coordinates (t, ϕ), with t the path length along the generating curve of the BOR from the lower pole, form an orthogonal curvilinear system on the surface S of the BOR; the corresponding unit vectors are $(\hat{\mathbf{t}}, \hat{\boldsymbol{\phi}})$. Figure 2 shows the propagation vector $\mathbf{k}^{inc} = k\,\hat{\mathbf{k}}^{inc}$ of the incident plane wave. The propagation vector is assumed to lie in the xz plane $(\phi = 0)$, with $-\hat{\mathbf{k}}^{inc}$ making an angle of θ^{inc} with the positive z axis and with $k_x^{inc} \leq 0$ so that

$$\mathbf{k}^{inc} = -k(\sin\theta^{inc}\hat{\mathbf{x}} + \cos\theta^{inc}\hat{\mathbf{z}}). \tag{10}$$

Also shown in Figure 2 are the spherical polar angles of the far field observation point $\mathbf{r}^{far} = (r, \theta^{far}, \phi^{far})$ and the associated unit vectors $\hat{\theta}^{far}$ and $\hat{\boldsymbol{\phi}}^{far}$. For TM illumination the incident electric field is given

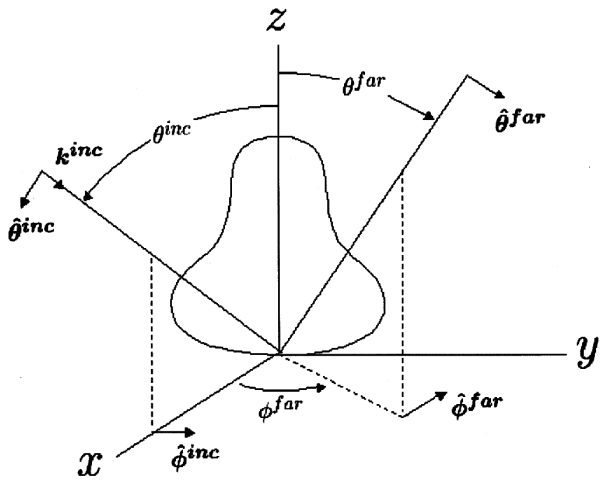

Figure 2. Plane wave scattering by a body of revolution.

by

$$\mathbf{E}^{inc} = kZ_0 \exp(-j\mathbf{k}^{inc} \cdot \mathbf{r})\hat{\theta}^{inc} \tag{11}$$

while for TE illumination it is given by

$$\mathbf{E}^{inc} = kZ_0 \exp(-j\mathbf{k}^{inc} \cdot \mathbf{r})\hat{\phi}^{inc}. \tag{12}$$

In (11) and (12) $\mathbf{r}$ is the vector from the origin to any point in space and the factor of kZ_0 is inserted to simplify the later expressions.

Thus, for a BOR (9) can be replaced by the equivalent pair of equations

$$j\hat{\mathbf{t}} \cdot \oint_S \left\{ \left[k^2 \mathbf{K}(\mathbf{r}') + \nabla'_S \left(\nabla'_S \cdot \mathbf{K}(\mathbf{r}') \right) + J' \left(\nabla'_S \cdot \mathbf{K}(\mathbf{r}') \right) \hat{\mathbf{n}}' \right] G(\mathbf{r}, \mathbf{r}') \right.$$
$$\left. - \left(\nabla'_S \cdot \mathbf{K}(\mathbf{r}') \right) \frac{\partial G(\mathbf{r}, \mathbf{r}')}{\partial n'} \hat{\mathbf{n}}' \right\} dS' = \frac{k}{Z_0} \hat{\mathbf{t}} \cdot \mathbf{E}^{inc}(\mathbf{r}) \tag{13a}$$

and

$$j\hat{\boldsymbol{\phi}} \cdot \oint_S \left\{ \left[k^2 \mathbf{K}(\mathbf{r}') + \nabla'_S \left(\nabla'_S \cdot \mathbf{K}(\mathbf{r}') \right) + J' \left(\nabla'_S \cdot \mathbf{K}(\mathbf{r}') \right) \hat{\mathbf{n}}' \right] G(\mathbf{r}, \mathbf{r}') \right.$$
$$\left. - \left(\nabla'_S \cdot \mathbf{K}(\mathbf{r}') \right) \frac{\partial G(\mathbf{r}, \mathbf{r}')}{\partial n'} \hat{\mathbf{n}}' \right\} dS' = \frac{k}{Z_0} \hat{\boldsymbol{\phi}} \cdot \mathbf{E}^{inc}(\mathbf{r}). \tag{13b}$$

The LEFIE for a PEC scatterer with a closed smooth surface in (9) and for closed smooth BORs in (13), like the original EFIE in

(1), produces a unique solution for the surface current $\mathbf{K}$ except at frequencies equal to the resonant frequencies of the cavity formed by the closed surface S of the scatterer. These spurious resonances can be eliminated from the LEFIE in the same way they have been eliminated from the EFIE. For example, the LEFIE can be combined with the magnetic-field integral equation [4] or added to a corresponding LEFIE that is satisfied on a dual surface just inside the surface S of the scatterer [5–9]. To concentrate on the subject of lowering the order of the singularity of the EFIE and not on the details of these methods for eliminating spurious resonances, we shall choose frequencies in our numerical examples that are sufficiently far from any cavity resonance to avoid numerical instabilities.

2.3. Solution of the LEFIE for a BOR by the Method of Moments

To solve the LEFIE (13) for the surface current, we begin by expanding $\mathbf{K}$ in a Fourier series

$$\mathbf{K}(t',\phi') = \sum_{n=-N}^{N} \left[K_n^t(t')\hat{\mathbf{t}}(t',\phi') + K_n^{\phi}(t')\hat{\boldsymbol{\phi}}(\phi')\right] e^{jn\phi'}. \tag{14}$$

The choice of the value of N is discussed in Subsection 2.4. To obtain separate integral equations for each of the Fourier modes we multiply both sides of (13a) and (13b) by $e^{-jm\phi}, m = 0, \pm 1, \pm 2, \cdots$, and integrate with respect to ϕ from $-\pi$ to π. As will be seen below, the integrands of the left-hand sides of (13a) and (13b) are of the form $F(t,t',\phi'-\phi)e^{jn\phi'}$ if the dot products of $\hat{\mathbf{t}}$ and $\hat{\boldsymbol{\phi}}$ are taken inside the integral signs. Noting that $dS' = \rho' dt' d\phi'$ and performing the integration with respect to ϕ' from $-\pi$ to π as well as the integration with respect to ϕ we then have

$$\begin{aligned}
&\int_{-\pi}^{\pi} d\phi e^{-jm\phi} \int_{-\pi}^{\pi} d\phi' e^{jn\phi'} F(t,t',\phi'-\phi) \\
&\quad = \int_{-\pi}^{\pi} d\phi e^{j(n-m)\phi} \int_{-\pi}^{\pi} d\phi' e^{jn(\phi'-\phi)} F(t,t',\phi'-\phi) \\
&\quad = 2\pi\delta_{nm} \int_{-\pi}^{\pi} d\phi' e^{jn\phi'} F(t,t',\phi')
\end{aligned} \tag{15}$$

where the Kronecker delta δ_{nm} equals 0 for $m \neq n$ and equals 1 for $m = n$. The orthogonality of the Fourier modes thus enables separate

integral equations to be obtained for each Fourier mode $e^{jn\phi}$.

Following the ϕ and ϕ' integrations we approximate $K_n^t(t')$ and $K_n^\phi(t')$ by pulse basis functions defined as follows. The generating curve of the BOR is parameterized in terms of t, the distance along the curve measured from the lower pole of the BOR. For each value of t, the corresponding point on the generating curve is given by $[\rho(t), z(t)]$. A set of $M+1$ points $p_1^\star, p_2^\star, \cdots, p_{M+1}^\star$ is chosen to discretize the generating curve with $p_1^\star = (\rho_1^\star, z_1^\star)$ being the lower pole of the generating curve corresponding to $t = 0$, and $p_{M+1}^\star = (\rho_{M+1}^\star, z_{M+1}^\star)$ being the upper pole of the generating curve. The generating curve is approximated by straight line segments between adjacent points. The midpoints of the approximating straight line segments are given by

$$(\rho_i, z_i) = \left(\frac{\rho_i^\star + \rho_{i+1}^\star}{2}, \frac{z_i^\star + z_{i+1}^\star}{2} \right), \quad i = 1, 2, \cdots, M \tag{16}$$

with the length of the i^{th} straight line segment denoted by

$$d_i = \left[\left(\rho_{i+1}^\star - \rho_i^\star\right)^2 + \left(z_{i+1}^\star - z_i^\star\right)^2 \right]^{1/2}. \tag{17}$$

For calculation purposes the discretized generating curve completely replaces the original generating curve and the parameter t now becomes the length along the discretized curve from the lower pole instead of the length along the original generating curve from the lower pole. Thus, for example, $t(p_1^\star) = 0$, $t(p_2^\star) = d_1$, $t(p_3^\star) = d_1 + d_2$, etc. A pulse basis function $p_i(t)$ is defined as

$$p_i(t) = \begin{cases} 0, & t \le t_i^\star, \ \ t \ge t_{i+1}^\star \\ 1, & t_i^\star \le t \le t_{i+1}^\star \end{cases} . \tag{18}$$

Then

$$K_n^t(t') \approx \sum_{i=1}^{M} K_n^t(t_i') p_i(t') \tag{19a}$$

and

$$K_n^\phi(t') \approx \sum_{i=1}^{M} K_n^\phi(t_i') p_i(t'). \tag{19b}$$

A set of $2M$ equations for the $2M$ unknowns $K_n^t(t_i), K_n^\phi(t_i), \ i = 1, 2, \cdots, M$, is then obtained by using point-matching: the left-hand side and right-hand side of the integral equations for each Fourier mode are equated at $t = t_i, \ i = 1, 2, \cdots, M$. This set of $2M$ equations can be expressed in matrix form as

$$\begin{bmatrix} [Z_n^{tt}] & [Z_n^{t\phi}] \\ [Z_n^{\phi t}] & [Z_n^{\phi\phi}] \end{bmatrix} \begin{bmatrix} \mathbf{K}_n^t \\ \mathbf{K}_n^\phi \end{bmatrix} = \begin{bmatrix} \mathbf{V}_n^t \\ \mathbf{V}_n^\phi \end{bmatrix}, \quad n = 0, \pm 1, \pm 2, \cdots, \pm N. \tag{20}$$

In (20) the $[Z_n^{pq}]$, $p, q = t$ or ϕ, are $M \times M$ matrices obtained from the left-hand sides of (13a) and (13b). The index p corresponds to the external dot product factor $\hat{\mathbf{t}}$ or $\hat{\boldsymbol{\phi}}$, and the index q corresponds to the t or ϕ component of $\mathbf{K}$. The i^{th} row of $[Z_n^{pq}]$ corresponds to the value of the observation point t_i, and the j^{th} column of $[Z_n^{pq}]$ corresponds to $K_n^q(t_j)$. The i^{th} value of the $M \times 1$ vectors $\mathbf{K_n^t}$ and $\mathbf{K_n^\phi}$ equals $K_n^t(t_i)$ and $K_n^\phi(t_i)$ respectively. The vectors $\mathbf{V_n^t}$ and $\mathbf{V_n^\phi}$ on the right-hand side of (20) contain the values of the right-hand sides of (13a) and (13b), respectively, evaluated at $t = t_i,\ i = 1, 2, \cdots, M$, following multiplication by $e^{-jn\phi}$ and integration with respect to ϕ from $-\pi$ to π.

A quadratic Lagrangian interpolation polynomial [10] is used to obtain the necessary approximations for both the first and second derivatives in (13), namely [11]

$$\frac{d}{dt'}\left[\rho' K_n^t(t')\right]_{t'=t_j} \approx \sum_{k=-1}^{1} c'_{j+k}\rho_{j+k}K^t_{n,j+k} \tag{21a}$$

$$\frac{d}{dt'}\left[\frac{1}{\rho'}K_n^\phi(t')\right]_{t'=t_j} \approx \sum_{k=-1}^{1} c'_{j+k}\frac{1}{\rho_{j+k}}K^\phi_{n,j+k} \tag{21b}$$

$$\frac{d^2}{dt'^2}\left[\rho' K_n^t(t')\right]_{t'=t_j} \approx \sum_{k=-1}^{1} c''_{j+k}\rho_{j+k}K^t_{n,j+k} \tag{21c}$$

where we have denoted $K_n^t(t_j)$ and $K_n^\phi(t_j)$ by $K^t_{n,j}$ and $K^\phi_{n,j}$ respectively. When $j = 1$ in (21), k is summed form 0 to 2; and when $j = M$ in (21), k is summed form -2 to 0. That is, one-sided finite-difference approximations to the derivatives are used at either end of the BOR.

Detailed expressions for the Z matrices, the $\mathbf{V}$ vectors, the surface currents $\mathbf{K}$, and the far scattered electric fields are given in Appendix A.

2.4. Number of Fourier Modes for Expansion and Testing Functions

The ϕ dependence of the current given by (14) is expressed as a summation from $-N$ to N of the Fourier modes $e^{jn\phi}$. The value of N can be set equal to the number of Fourier modes sufficient to represent (to the desired accuracy) the ϕ variation of the tangential component of the incident electric field on the surface of the BOR. Let a be the

largest value of ρ of a point (ρ, z) on the generating curve of the BOR. Then from (10)–(12) it can be seen that the ϕ variation of the incident field along the circle on the BOR corresponding to the point (a, z) is given by

$$f(\phi) = \cos\phi e^{jka\sin\theta^{inc}\cos\phi} \quad \text{or} \quad f(\phi) = \sin\phi e^{jka\sin\theta^{inc}\cos\phi}. \tag{22}$$

For axial incidence $\theta^{inc} = 0$ and $f(\phi)$ equals $\cos\phi$ or $\sin\phi$ so that only the $e^{\pm j\phi}$ modes are excited. For oblique incidence, we can express $f(\phi)$ as the Fourier series

$$f(\phi) = \sum_{-N}^{N} c_n e^{jn\phi} \tag{23a}$$

such that

$$c_n = \frac{1}{2\pi}\int_0^{2\pi} f(\phi)e^{-jn\phi}d\phi. \tag{23b}$$

With the help of (22) and the definition of the Bessel function, we find

$$\mid c_n \mid = \frac{1}{2}\left|J_{n+1}(ka\sin\theta^{inc}) \pm J_{n-1}(ka\sin\theta^{inc})\right|. \tag{24}$$

As n increases beyond $ka\sin\theta^{inc}$, $J_n(ka\sin\theta^{inc})$ decreases rapidly and it suffices to choose

$$N = I + M \tag{25}$$

where

$$I = \mathrm{Int}[(1+\alpha)ka\sin\theta^{inc}], \quad 0 < \alpha \ll 1 \tag{26}$$

and M is the smallest integer for which

$$\frac{J_N(ka\sin\theta^{inc})}{J_I(ka\sin\theta^{inc})} \leq \epsilon \tag{27}$$

with ϵ a small positive number depending on the desired accuracy. If the value of N given by (25) is plotted as a function of $\mathrm{Int}[ka\sin\theta^{inc}]$, the plot is found to be almost linear. For $\epsilon = 0.005$, for example,

$$N \approx \mathrm{Int}[1.04ka\sin\theta^{inc}] + 7. \tag{28}$$

A similar expression

$$N \approx \mathrm{Int}[k^{+}(a\sin\theta) + \lambda] \tag{29}$$

with k^{+} denoting a value a few percent larger than k was obtained by Yaghjian [13] for the reciprocal problem of estimating the number of angular modes needed to represent the far field of a radiator in the θ direction.

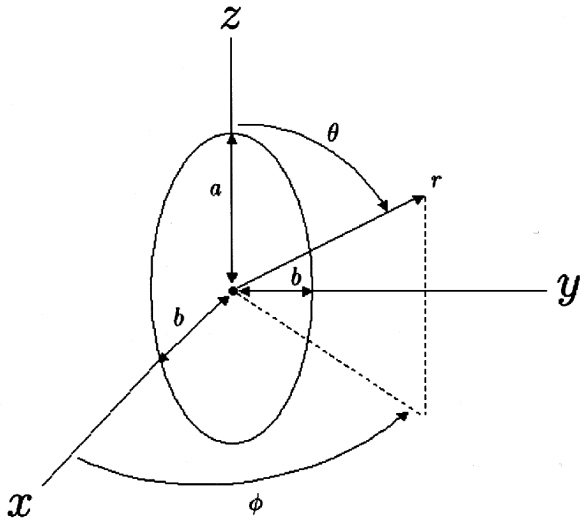

Figure 3. Geometry of the prolate spheroid.

3. NUMERICAL RESULTS

The analysis presented in Section 2 was implemented in a FORTRAN computer program which was then used to obtain numerical results for several different BORs. In this section we show some representative results using the LEFIE to calculate scattering from a prolate spheroid. The geometry of the spheroid is shown in Figure 3. The semi-major axis of the spheroid is a and the semi-minor axis is b. For the calculations we show, $ka = 20$ and $kb = 10$. The TM illuminating plane wave makes an angle of 45° with the major axis of the spheroid. For these values of ka and kb, no spurious resonances are encountered; see end of Subsection 2.2.

The solid curve in Figure 4 shows the E-plane radar cross section (RCS) pattern calculated with the combined field integral equation (CFIE) implemented in the computer code CICERO [14] using a discretization of the spheroid generating curve of 40 points/λ. The dotted curve in Figure 4 is the pattern obtained by solving the conventional EFIE with the Galerkin form of the method of moments and overlapping triangle basis functions with a point density of 20 points/λ. The dot-dashed curve and the dashed curve in Figure 4 are the patterns obtained solving the conventional EFIE with pulse basis functions and point matching at point densities of 20 points/λ and 80 points/λ, respectively. We note that the CFIE and EFIE solved with

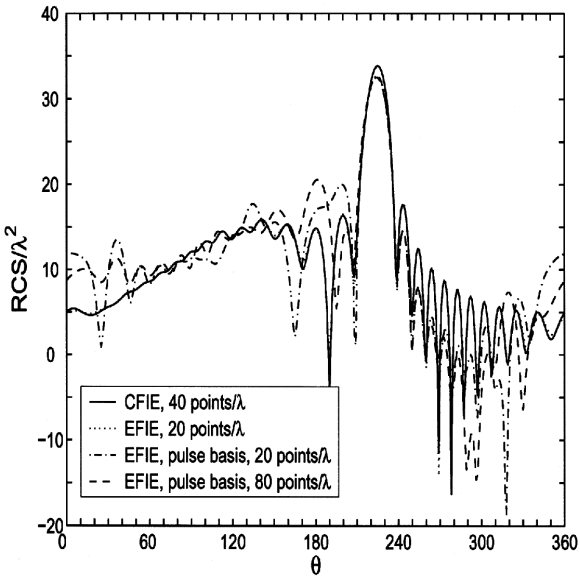

Figure 4. E-plane pattern of a prolate spheroid with $ka = 20$ and $kb = 10$ illuminated by a TM plane wave incident at an angle of 45° with the major axis, as calculated by the CFIE with a density of 40 points/λ, by the EFIE solved with overlapping triangle basis functions at a density of 20 points/λ, and by the EFIE solved with pulse basis functions and point matching at a density of 20 points/λ and 80 points/λ.

overlapping triangle basis functions yield results that agree closely, but the patterns obtained with pulse basis functions and point matching are highly inaccurate. Moreover, these pulse basis function patterns are not significantly improved upon by considerably increasing the point density.

In contrast with the very poor results obtained when the conventional EFIE is solved using pulse basis functions and point matching, in Figure 5 we show the spheroid patterns obtained solving the conventional EFIE with the method of moments and overlapping triangle basis functions with a density of 20 points/λ, and the patterns obtained by solving the LEFIE with pulse basis functions and point matching at densities of 40 pointsλ and 20 points/λ. The LEFIE solved at a density of 40 points/λ yields a pattern quite close to the conventional EFIE pattern obtained at a density of 20 points/λ. The LEFIE solved with a density of 20 points/λ, however, has some pattern

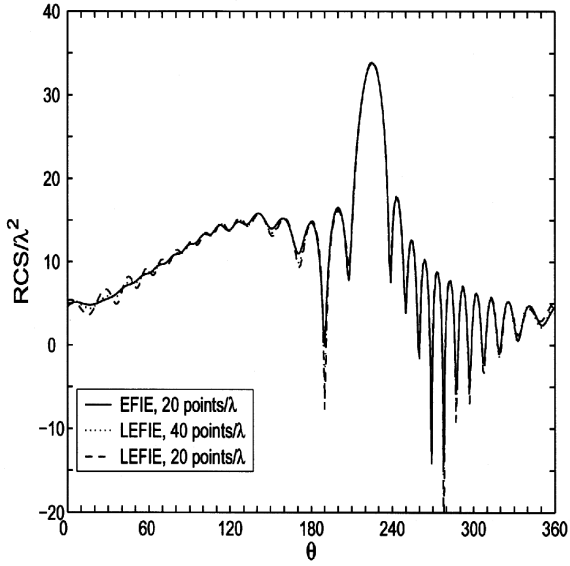

Figure 5. E-plane pattern of a prolate spheroid with $ka = 20$ and $kb = 10$ illuminated by a TM plane wave incident at an angle of 45° with the major axis, as calculated by the EFIE solved with overlapping triangle basis functions at a density of 20 points/λ, and by the LEFIE solved with pulse basis functions and point matching at a density of 40 points/λ and 20 points/λ.

errors of approximately 1.5 dB. The point density required to obtain results with the LEFIE comparable in accuracy to those obtained with the conventional EFIE can be improved upon considerably by the stratagem of using a higher point density for only a very small region – say $\lambda/4$ – in the vicinity of the ends of the spheroid generating curve, and a low point density elsewhere as shown in Figure 6. In the LEFIE pattern shown in Figure 6 a density of 80 points/λ was used close to the ends of the spheroid generating curve (i.e., the poles of the spheroid) and a density of 20 points/λ was used elsewhere. The reason why a high point density may be required at the ends of the BOR generating curve is that the finite-difference approximation of the first and second derivatives used in solving the LEFIE is less accurate at the beginning and end of the generating curve because one-sided derivative approximations must be used there; see (21). Using a higher point density at the ends of the generating curve compensates for the use of the one-sided finite-difference derivative approximations.

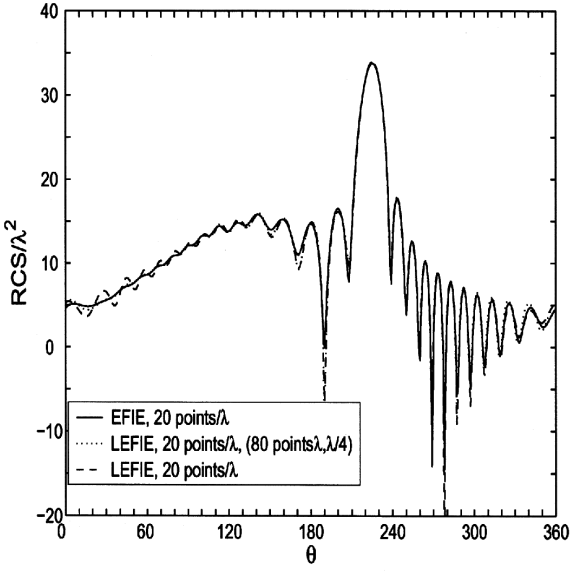

Figure 6. E-plane pattern of a prolate spheroid with $ka = 20$ and $kb = 10$ illuminated by a TM plane wave incident at an angle of 45° with the major axis, as calculated by the EFIE solved with overlapping triangle basis functions at a density of 20 points/λ, by the LEFIE solved with pulse basis functions and point matching at a density of 80 points/λ in an interval of $\lambda/4$ at either end of the spheroid generating curve and 20 points/λ elsewhere, and by the LEFIE at a uniform density of 20 points/λ.

4. SUMMARY

Unlike the magnetic-field integral equation, the conventional form of the electric-field integral equation cannot be solved accurately using pulse-basis functions and point matching. Moreover, it can be demonstrated that it is the highly singular kernel of the EFIE, rather than the derivatives of the current, that precludes the use of the pulse-basis-function point-matching MOM. A new form of the EFIE has been derived whose kernel has no greater singularity than the free-space Green's function. This new low-order-singularity form of the EFIE, the LEFIE, has been applied to a perfectly electrically conducting body of revolution using a pulse-basis function point-matching MOM, and a computer program has been written to implement the numerical solution. Derivatives of the current are approximated with finite

differences using a quadratic Lagrangian interpolation polynomial. Such a simple solution of the LEFIE is contingent, however, upon the vanishing of a linear integration term that appears when the original EFIE is transformed to obtain the LEFIE. The vanishing of this linear integration term restricts the applicability of the LEFIE to smooth closed scatterers without tips, edges, or any other features that might result in a discontinuous or unbounded surface charge density, its surface derivative, and the sum of the reciprocals of the principal radii of curvature, or a discontinuous unit normal vector to the surface. Bistatic RCS calculations performed for a prolate spheroid demonstrate that results comparable in accuracy to the conventional EFIE results (obtained with a triangular-function Galerkin MOM) can be obtained with the LEFIE using pulse-basis functions and point matching provided that a higher density of points is used close to the ends of the BOR generating curve to compensate for the use of one-sided finite difference approximations of the first and second derivatives of the current.

APPENDIX A. DETAILED EXPRESSIONS FOR THE Z MATRICES, THE V VECTORS, SURFACE CURRENTS K, AND FAR SCATTERED FIELDS

The Z_n^{pq} matrices in (20) can be expressed as the sum of four submatrices corresponding to each of the four terms under the integral signs in the LEFIE (13) [11]

$$[Z_n^{pq}] = [Z_n^{pq}]_1 + [Z_n^{pq}]_2 + [Z_n^{pq}]_3 + [Z_n^{pq}]_4\,, \quad p,q = t \text{ or } \phi \tag{A1}$$

where

$$\begin{aligned}
[Z_n^{tt}]_{1;ij} &= jk^2 d_j[\sin v_i \sin v_j G_{2,n}(\rho_i,\rho_j,z_i-z_j) \\
&\quad + \cos v_i \cos v_j G_{1,n}(\rho_i,\rho_j,z_i-z_j)] \\
[Z_n^{\phi t}]_{1;ij} &= -k^2 d_j \rho_j \sin v_j G_{3,n}(\rho_i,\rho_j,z_i-z_j) \\
[Z_n^{t\phi}]_{1;ij} &= k^2 d_j \rho_j \sin v_i G_{3,n}(\rho_i,\rho_j,z_i-z_j) \\
[Z_n^{\phi\phi}]_{1;ij} &= jk^2 d_j G_{2,n}(\rho_i,\rho_j,z_i-z_j)
\end{aligned} \tag{A2}$$

$$\begin{aligned}
[Z_n^{tt}]_{2;i,j+k} &= jd_j\rho_j\,[\sin v_i \sin v_j G_{2,n}(\rho_i,\rho_j,z_i-z_j) \\
&\quad + \cos v_i \cos v_j G_{1,n}(\rho_i,\rho_j,z_i-z_j)] \\
&\quad \times \left(\frac{1}{\rho_j} c''_{j+k}\rho_{j+k} - \frac{1}{\rho_j^2}\sin v_j c'_{j+k}\rho_{j+k}\right)
\end{aligned}$$

$$
\begin{aligned}
&+ jn \sin v_i d_j G_{3,n}(\rho_i, \rho_j, z_i - z_j) \frac{1}{\rho_j^2} c''_{j+k} \rho_{j+k} \\
[Z_n^{\phi t}]_{2;i,j+k} &= -d_j \rho_j \sin v_j G_{3,n}(\rho_i, \rho_j, z_i - z_j) \\
&\times \left(\frac{1}{\rho_j} c''_{j+k} \rho_{j+k} - \frac{1}{\rho_j^2} \sin v_j c'_{j+k} \rho_{j+k} \right) \\
&- nd_j G_{2,n}(\rho_i, \rho_j, z_i - z_j) c'_{j+k} \rho_{j+k} \\
[Z_n^{t\phi}]_{2;i,j+k} &= -nd_j \rho_j \left[\sin v_i \sin v_j G_{2,n}(\rho_i, \rho_j, z_i - z_j) \right. \\
&\left. + \cos v_i \cos v_j G_{1,n}(\rho_i, \rho_j, z_i - z_j) \right] c'_{j+k} \frac{1}{\rho_{j+k}} \\
&- n^2 \frac{d_j}{\rho_j} \sin v_i G_{3,n}(\rho_i, \rho_j, z_i - z_j) \mid_{k=0} \\
[Z_n^{\phi\phi}]_{2;i,j} &= -jnd_j \rho_j \sin v_j G_{3,n}(\rho_i, \rho_j, z_i - z_j) \\
&- jn^2 \frac{d_j}{\rho_j} G_{2,n}(\rho_i, \rho_j, z_i - z_j)
\end{aligned} \tag{A3}
$$

$$
\begin{aligned}
[Z_n^{tt}]_{3;i,j+k} &= jd_j J(t_j) [\sin v_i \cos v_j G_{2,n}(\rho_i, \rho_j, z_i - z_j) \\
&- \cos v_i \sin v_j G_{1,n}(\rho_i, \rho_j, z_i - z_j)] c'_{j+k} \rho_{j+k} \\
[Z_n^{\phi t}]_{3;i,j+k} &= -d_j J(t_j) \cos v_j G_{3,n}(\rho_i, \rho_j, z_i - z_j) c'_{j+k} \rho_{j+k} \\
[Z_n^{t\phi}]_{3;i,j} &= -nd_j J(t_j) [\sin v_i \cos v_j G_{2,n}(\rho_i, \rho_j, z_i - z_j) \\
&- \cos v_i \sin v_j G_{1,n}(\rho_i, \rho_j, z_i - z_j)] \\
[Z_n^{\phi\phi}]_{3;i,j} &= -jnd_j J(t_j) \cos v_j G_{3,n}(\rho_i, \rho_j, z_i - z_j)
\end{aligned} \tag{A4}
$$

$$
\begin{aligned}
[Z_n^{tt}]_{4;i,j+k} &= -jk^2 d_j [\rho_i \sin v_i \cos^2 v_j H_{4,n}(\rho_i, \rho_j, z_i - z_j) \\
&- \rho_i \cos v_i \cos v_j \sin v_j H_{2,n}(\rho_i, \rho_j, z_i - z_j) \\
&- \rho_j \sin v_i \cos^2 v_j H_{2,n}(\rho_i, \rho_j, z_i - z_j) \\
&+ \rho_j \cos v_i \cos v_j \sin v_j H_{1,n}(\rho_i, \rho_j, z_i - z_j) \\
&- (z_i - z_j)(\sin v_i \cos v_j \sin v_j H_{2,n}(\rho_i, \rho_j, z_i - z_j) \\
&- \cos v_i \sin^2 v_j H_{1,n}(\rho_i, \rho_j, z_i - z_j))] c'_{j+k} \rho_{j+k} \\
[Z_n^{\phi t}]_{4;i,j+k} &= k^2 d_j [\rho_i \cos^2 v_j H_{5,n}(\rho_i, \rho_j, z_i - z_j) \\
&- \rho_i \cos^2 v_j H_{3,n}(\rho_i, \rho_j, z_i - z_j) \\
&- (z - z') \cos v_j \sin v_j H_{3,n}(\rho_i, \rho_j, z_i - z_j)] c'_{j+k} \rho_{j+k} \\
[Z_n^{t\phi}]_{4;i,j} &= nk^2 d_j [\rho_i \sin v_i \cos^2 v_j H_{4,n}(\rho_i, \rho_j, z_i - z_j) \\
&- \rho_i \cos v_i \cos v_j \sin v_j H_{2,n}(\rho_i, \rho_j, z_i - z_j)
\end{aligned}
$$

$$
\begin{aligned}
&- \rho_j \sin v_i \cos^2 v_j H_{2,n}(\rho_i, \rho_j, z_i - z_j) \\
&+ \rho_j \cos v_i \cos v_j \sin v_j H_{1,n}(\rho_i, \rho_j, z_i - z_j) \\
&- (z_i - z_j)(\sin v_i \cos v_j \sin v_j H_{2,n}(\rho_i, \rho_j, z_i - z_j) \\
&- \cos v_i \sin^2 v_j H_{1,n}(\rho_i, \rho_j, z_i - z_j))] \\
[Z_n^{\phi\phi}]_{i,j} &= jk^2 n d_j [\rho_i \cos^2 v_j H_{5,n}(\rho_i, \rho_j, z_i - z_j) \\
&- \rho_i \cos^2 v_j H_{3,n}(\rho_i, \rho_j, z_i - z_j) \\
&- (z_i - z_j) \cos v_j \sin v_j H_{3,n}(\rho_i, \rho_j, z_i - z_j) \qquad \text{(A5)}
\end{aligned}
$$

with

$$
\begin{aligned}
G_{1,n}(\rho, \rho', z - z') &= \int_0^\pi G_0(R) \cos(n\phi') d\phi' \\
G_{2,n}(\rho, \rho', z - z') &= \int_0^\pi G_0(R) \cos(n\phi') \cos\phi' d\phi' \\
G_{3,n}(\rho, \rho', z - z') &= \int_0^\pi G_0(R) \sin(n\phi') \sin\phi' d\phi' \\
G_0(R) &= \frac{\exp(-jkR)}{kR} \qquad \text{(A6)}
\end{aligned}
$$

and

$$
\begin{aligned}
H_{1,n}(\rho, \rho', z - z') &= \int_0^\pi H_0(R) \cos(n\phi') d\phi' \\
H_{2,n}(\rho, \rho', z - z') &= \int_0^\pi H_0(R) \cos(n\phi') \cos\phi' d\phi' \\
H_{3,n}(\rho, \rho', z - z') &= \int_0^\pi H_0(R) \sin(n\phi') \sin\phi' d\phi' \\
H_{4,n}(\rho, \rho', z - z') &= \int_0^\pi H_0(R) \cos(n\phi') \cos^2\phi' d\phi' \\
H_{5,n}(\rho, \rho', z - z') &= \int_0^\pi H_0(R) \sin(n\phi') \cos\phi' \sin\phi' d\phi' \\
H_0(R) &= \frac{1 + jkR}{(kR)^3} \exp(-jkR). \qquad \text{(A7)}
\end{aligned}
$$

The angles v and v' are measured positive clockwise from the positive z axis to $\hat{\mathbf{t}}$ and $\hat{\mathbf{t}}'$, respectively, and their discretized values are given by

$$\sin v_i = \frac{\rho^\star_{i+1} - \rho^\star_i}{d_i}, \quad \cos v_i = \frac{z^\star_{i+1} - z^\star_i}{d_i}. \tag{A8}$$

We find that the following relationships hold

$$[Z^{tt}_{-n}] = [Z^{tt}_n], \quad [Z^{t\phi}_{-n}] = -[Z^{t\phi}_n], \quad [Z^{\phi t}_{-n}] = -[Z^{\phi t}_n], \quad [Z^{\phi\phi}_{-n}] = [Z^{\phi\phi}_n]. \tag{A9}$$

Similarly, the components of the $\mathbf{V}^t_n$ and $\mathbf{V}^\phi_n$ vectors can be expressed as [11]

$$\begin{aligned}
V^{t\theta}_{ni} &= \pi j^{n+1} k \left[\cos\theta^{inc} \sin v_i (J_{n+1} - J_{n-1}) + 2j \sin\theta^{inc} \cos v_i J_n\right] \\
&\quad \times e^{jkz_i \cos\theta^{inc}} \\
V^{\phi\theta}_{ni} &= \pi j^n k \cos\theta^{inc} (J_{n+1} + J_{n-1}) e^{jkz_i \cos\theta^{inc}} \\
V^{t\phi}_{ni} &= -\pi j^n k \sin v_i (J_{n+1} + J_{n-1}) e^{jkz_i \cos\theta^{inc}} \\
V^{\phi\phi}_{ni} &= \pi j^{n+1} k (J_{n+1} - J_{n-1}) e^{jkz_i \cos\theta^{inc}}
\end{aligned} \tag{A10}$$

where $J_n = J_n(k\rho_i \sin\theta^{inc})$ denotes the Bessel functions, and the following relationships hold

$$V^{t\theta}_{-ni} = V^{t\theta}_{ni}, \quad V^{\phi\theta}_{-ni} = -V^{\phi\theta}_{ni}, \quad V^{t\phi}_{-ni} = -V^{t\phi}_{ni}, \quad V^{\phi\phi}_{-ni} = V^{\phi\phi}_{ni}. \tag{A11}$$

The expressions for the currents induced on the surface of the BOR by a TM and TE linearly polarized incident plane wave are given, respectively, by [11]

$$\begin{aligned}
\mathbf{K}^\theta(t,\phi) &= \tilde{p}\mathbf{K}^{t\theta}_0 \hat{\mathbf{t}}(t,\phi) \\
&\quad + 2\sum_{n=1}^{N} \left[(\tilde{p}\mathbf{K}^{t\theta}_n) \cos n\phi \hat{\mathbf{t}} + j(\tilde{p}\mathbf{K}^{\phi\theta}_n) \sin n\phi \hat{\boldsymbol{\phi}}(\phi)\right] \\
\mathbf{K}^\phi(t,\phi) &= \tilde{p}\mathbf{K}^{\phi\phi}_0 \hat{\boldsymbol{\phi}} \\
&\quad + 2\sum_{n=1}^{N} \left[(\tilde{p}\mathbf{K}^{t\phi}_n) \sin n\phi \hat{\mathbf{t}}(t,\phi) + (\tilde{p}\mathbf{K}^{\phi\phi}_n) \cos n\phi \hat{\boldsymbol{\phi}}(\phi)\right]
\end{aligned} \tag{A12}$$

where $\tilde{p} = [p_1(t), p_2(t), \cdots p_N(t)]$ and the following relationships hold

$$\mathbf{K}^{t\theta}_{-n} = \mathbf{K}^{t\theta}_n, \quad \mathbf{K}^{\phi\theta}_{-n} = -\mathbf{K}^{\phi\theta}_n, \quad \mathbf{K}^{t\phi}_{-n} = -\mathbf{K}^{t\phi}_n, \quad \mathbf{K}^{\phi\phi}_{-n} = \mathbf{K}^{\phi\phi}_n. \tag{A13}$$

Finally, the expressions for the components of the far scattered electric field are given by [11]

$$\begin{aligned}
E^{sc,\theta\theta}(\mathbf{r}) &\overset{r\to\infty}{\sim} -\frac{jkZ_0e^{-jkr}}{4\pi kr} \\
&\quad\times \left[\tilde{\mathbf{R}}_0^{t\theta}\mathbf{K}_0^{t\theta} + 2\sum_{n=1}^{N}\left(\tilde{\mathbf{R}}_n^{t\theta}\mathbf{K}_n^{t\theta} + \tilde{\mathbf{R}}_n^{\phi\theta}\mathbf{K}_n^{\phi\theta}\right)\cos(n\phi^{far})\right] \\
E^{sc,\phi\theta}(\mathbf{r}) &\overset{r\to\infty}{\sim} \frac{kZ_0e^{-jkr}}{4\pi kr}2\sum_{n=1}^{N}\left(\tilde{\mathbf{R}}_n^{t\phi}\mathbf{K}_n^{t\theta} + \tilde{\mathbf{R}}_n^{\phi\phi}\mathbf{K}_n^{\phi\theta}\right)\sin(n\phi^{far}) \\
E^{sc,\theta\phi}(\mathbf{r}) &\overset{r\to\infty}{\sim} \frac{kZ_0e^{-jkr}}{4\pi kr}2\sum_{n=1}^{N}\left(\tilde{\mathbf{R}}_n^{t\theta}\mathbf{K}_n^{t\phi} + \tilde{\mathbf{R}}_n^{\phi\theta}\mathbf{K}_n^{\phi\phi}\right)\sin(n\phi^{far}) \\
E^{sc,\phi\phi}(\mathbf{r}) &\overset{r\to\infty}{\sim} -\frac{jkZ_0e^{-jkr}}{4\pi kr} \\
&\quad\times \left[\tilde{\mathbf{R}}_0^{\phi\phi}\mathbf{K}_0^{\phi\phi} + 2\sum_{n=1}^{N}\left(\tilde{\mathbf{R}}_n^{t\phi}\mathbf{K}_n^{t\phi} + \tilde{\mathbf{R}}_n^{\phi\phi}\mathbf{K}_n^{\phi\phi}\right)\cos(n\phi^{far})\right]
\end{aligned} \tag{A14}$$

with

$$\begin{aligned}
R_{ni}^{t\theta} &= \pi j^{n+1}kd_i\rho_i \\
&\quad\times \left[\cos\theta^{far}\sin v_i(J_{n+1}^f - J_{n-1}^f) + 2j\sin\theta^{far}\cos v_i J_n^f\right] \\
&\quad\times e^{jkz_i\cos\theta^{far}} \\
R_{ni}^{\phi\theta} &= -\pi j^n kd_i\rho_i\cos\theta^{far}(J_{n+1}^f + J_{n-1}^f)e^{jkz_i\cos\theta^{far}} \\
R_{ni}^{t\phi} &= \pi j^n kd_i\rho_i\sin v_i(J_{n+1}^f + J_{n-1}^f)e^{jkz_i\cos\theta^{far}} \\
R_{ni}^{\phi\phi} &= \pi j^{n+1}kd_i\rho_i(J_{n+1}^f - J_{n-1}^f)e^{jkz_i\cos\theta^{far}} \\
J_n^f &= J_n(k\rho_i\sin\theta^{far})
\end{aligned} \tag{A15}$$

which obey the relationships

$$R_{-ni}^{t\theta} = R_{ni}^{t\theta}, \quad R_{-ni}^{\phi\theta} = -R_{ni}^{\phi\theta}, \quad R_{-ni}^{t\phi} = -R_{ni}^{t\phi}, \quad R_{-ni}^{\phi\phi} = R_{ni}^{\phi\phi}. \tag{A16}$$

The radar cross section σ is defined as

$$\sigma^{pq} = \lim_{r\to\infty} 4\pi r^2 \frac{|\, E^{sc,pq}\,|^2}{|\,\mathbf{E}^{inc,q}\,|^2} \tag{A17}$$

where $p:\theta$ or ϕ, denotes the component of the far scattered field, and $q:\theta$ (TM) or ϕ (TE), indicates the polarization of the incident electric field.

ACKNOWLEDGMENT

This work was supported by the U.S. Air Force Office of Scientific Research (AFOSR).

REFERENCES

1. Maue, A. W., "On the formulation of a general scattering problem by means of an integral equation," *Z. Phys.*, Vol. 126, 601–618, 1949.
2. Van Bladel, J., *Electromagnetic Fields*, McGraw-Hill, New York, 1964.
3. Yaghjian, A. D., "Augmented electric- and magnetic-field integral equations," *Radio Science*, Vol. 16, 987–1001, November–December 1981.
4. Mautz, J. R. and R. F. Harrington, "H-field, E-field, and combined-field solutions for conducting bodies of revolution," *Arch. Math. Ubertragungtech.*, Vol. 32, 157–164, 1978.
5. Yaghjian, A. D. and M. B. Woodworth, "Derivation, application and conjugate gradient solution of the dual-surface integral equations for three-dimensional, multiwavelength perfect conductors," *Progress in Electromagnetics Research*, PIER 5, T. Sarkar (ed.), Applications of the Conjugate Gradient Method to Electromagnetics and Signal Analysis, 103–130, Elsevier, New York, 1991.
6. Woodworth M. B. and A. D. Yaghjian, "Multiwavelength three-dimensional scattering with dual-surface integral equations," *J. Opt. Soc. Am. A*, Vol. 11, 1399–1413, April 1994.
7. Peterson, A. F., S. L. Ray, and R. Mittra, *Computational Methods for Electromagnetics*, IEEE Press, New York, 1998.
8. Shore, R. A. and A. D. Yaghjian, "Dual surface electric field equation," Air Force Research Laboratory Report, No. AFRL-SN-HS-TR-2001-013, 2001.
9. Shore, R. A. and A. D. Yaghjian,"Dual-surface integral equations in electromagnetic scattering," *Proceedings International Union of Radio Science (URSI) 27th General Assembly*, Maastricht, The Netherlands, August 2002.
10. Pearson, C. E., *Numerical Methods in Engineering and Science*, Van Nostrand Reinhold, New York, 1986.
11. Shore, R. A. and A. D. Yaghjian, "A low-order-singularity electric-field integral equation solvable with pulse basis functions and point matching," AFRL Technical Report, Hanscom AFB, MA, 2004 (PDF file available on request).

12. Balanis, C. A., *Advanced Engineering Electromagnetics*, John Wiley, New York, 1989.
13. Yaghjian, A. D., "Near field antenna measurements on a cylindrical surface: A source scattering matrix formulation," NBS Technical Note, No. 696, 1977.
14. Putnam, J. M. and L. N. Medgyesi-Mitschang, "Combined field integral equation formulation for axially inhomogeneous bodies of revolution," McDonnell Douglas Research Laboratories MDC Report, No. QA003, December 1987.

Robert A. Shore received the B.A. degree from Amherst College, Amherst, MA in 1957, and the M.A. and Ph.D. degrees in applied mathematics from Harvard University, Cambridge, MA in 1961 and 1967. He worked at the Air Force Cambridge Research Laboratory, Bedford, MA, from 1959 to 1969, at Israel Aircraft Company, Israel, from 1970 to 1974, and at Energy Resources Co., Cambridge, MA, from 1975 to 1979. Since 1979 he has been employed as a research physicist at the Electromagnetics Directorate of the Air Force Research Laboratory, Hanscom AFB, MA, where his research interests include adaptive antennas, computational electromagnetics, and high-frequency electromagnetic diffraction.

Arthur D. Yaghjian received the B.S., M.S., and Ph.D. degrees in electrical engineering from Brown University, Providence, RI in 1964, 1966, and 1969. After teaching for a year at Hampton Institute, VA, he joined the research staff of the Electromagnetics Division of the National Bureau of Standards, Boulder, CO. He transferred in 1983 to the Electromagnetics Directorate of the Air Force Research Laboratory, Hanscom AFB, MA, where he was employed as a research scientist until 1996. He presently works as an independent consultant in electromagnetics. His research interests include electromagnetic fields in continuous media; exact, numerical, and high-frequency methods for predicting and measuring the near and far fields of antennas and scatterers; and the classical equations of motion of charged particles.